Experimental Study of Stall Behavior in Radial Vaneless Diffuser of Centrifugal Pump

Yakushijin, Hirokazu
Department of Mechanical Engineering Science : Guraduate Student

Watanabe, Satoshi
Department of Mechanical Engineering Science : Associate Professor

Takahara, Hisasada
Department of Mechanical Engineering Science : Research Associate

Furukawa, Akinori
Department of Mechanical Engineering Science : Professor

Experimental Study of Stall Behavior in Radial Vaneless Diffuser of Centrifugal Pump

by

Hirokazu YAKUSHIJIN*, Satoshi WATANABE**

Hisasada TAKAHARA*** and Akinori FURUKAWA****

Abstract

A rotating stall phenomenon in radial vaneless diffuser of centrifugal pump has been investigated experimentally as the first stage of developing a method to suppress the stall. The test impeller is two-dimensional having six blades with outlet angles of 18.1 degrees and the diffuser is parallel walled with the outer diameter ratio of 1.90 to the impeller outlet and the height of 30 mm, which is the same of the impeller. Measured results are shown and discussed in the present paper as follows. The onset of rotating stall is triggered by a reverse flow occurring on the hub surface near the diffuser outlet. At that time the average angle of absolute flow velocity becomes less than 11.9 degrees at the section just downstream of the impeller. As the observed behaviors of rotating stall, change of stall cell numbers, amplitude and frequency of pressure fluctuation are clarified.

Keywords: Centrifugal pump, Vaneless diffuser, Static head recovery, Rotating stall

1. Introduction

The operation range of centrifugal type of turbomachinery is often restricted due to a rotating stall occurring in a radial diffuser at low flow rates[1],[2]. Since a rotating stall might cause unstable flow and piping system vibration, lots of researchers and engineers have made their efforts to elucidate the stall mechanism and to suppress the stall occurring. The adoptions of rough wall[3] and grooved wall[4] as passive methods and the installations of speaker[5] and air jet nozzle[6] on diffuser wall as active ones have been proposed to suppress the stall. These methods are effective but still insufficient for complete suppression over the

* Graduate Student, Department of Mechanical Engineering Science
** Associate Professor, Department of Mechanical Engineering Science
*** Research Associate, Department of Mechanical Engineering Science
**** Professor, Department of Mechanical Engineering Science

whole flow rate range. The final goal of the authors' study is to develop more effective method with a simple structure. At the first stage of the authors' study it is important to clarify the characteristics of a rotating stall phenomenon in radial vaneless diffuser. The test diffuser, installed downstream of a two-dimensional impeller with six blades of outlet angles of 18.1 degrees, is parallel walled with the outer diameter ratio of 1.90 to the impeller outlet and the height of 30 mm which is identical to that of the impeller. The shroud wall pressure and its fluctuation were measured with high response pressure sensors and two-dimensional flow distributions were also measured with a cobra-type three-holes yaw-meter at three radial sections. The measured results are shown and the appearance and the behaviors of the rotating stall are discussed with considering the relationship between the degree of static head recovery and the reverse flow occurring and that between the rotating stall phenomena and the appearance of reverse flow region.

2. Experimental Apparatus

Figure 1 shows the sectional view of the pump equipment with a vertical-rotating shaft. Water flows into the impeller ① through a Venturi flow-meter and boost pump from an open tank. Then water is discharged to a parallel walled diffuser ② with the height of $b=30$ mm which is the same as the impeller blade height, overflows after forming a free surface in axisymmetric channel ③ and returns to the open tank. In the present experiment, an oil seal is attached on the pump suction cover-ring to prevent a flow from returning from the impeller outlet to the inlet through a space between the impeller shroud and the casing. **Figure 2** shows the shape of the test impeller, which is a closed one with six two-dimensional blades of the inlet and outlet diameters of 200, 400 mm, respectively. This impeller has the suction and pressure surface blade outlet angles of $\beta_{b2s}=\beta_{b2p}=18.1$ degrees and the peripheral thickness of $t_{u2}=35.0$ mm at the outlet. In the present experiment the pump impeller speed was always kept at $N=200$ rpm.

The wall static pressures, at nine positions of different radius ratio to impeller outlet radius $R=r/r_2=1.02$, 1.03, 1.05, 1.06, 1.10, 1.15, 1.28, 1.50 and 1.80 on the diffuser wall of the
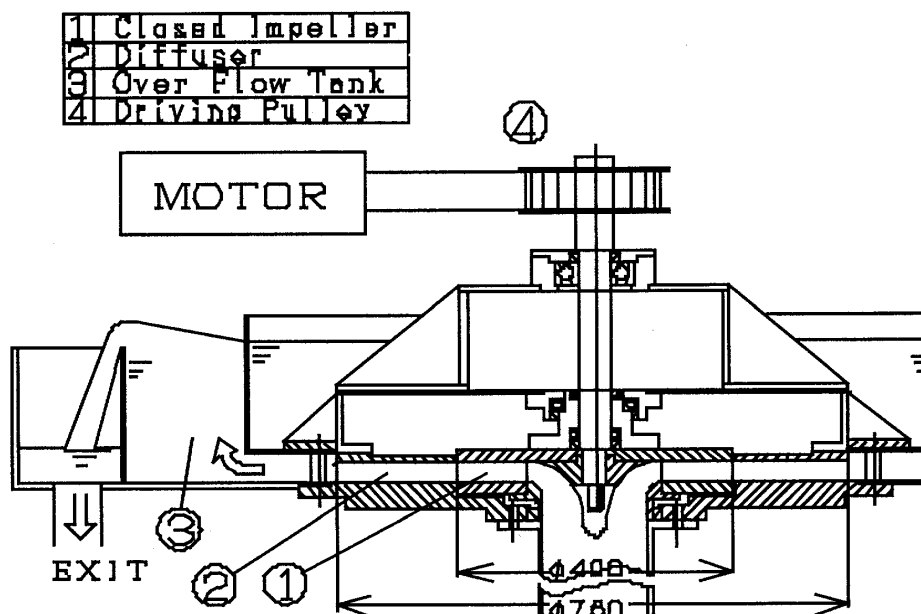

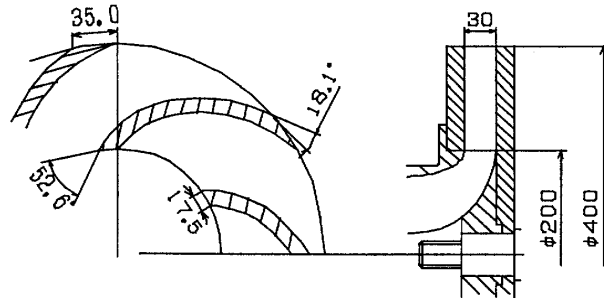| 1 | Closed Impeller |
2	Diffuser
3	Over Flow Tank
4	Driving Pulley

Fig. 1 Sectional view of pump equipment.
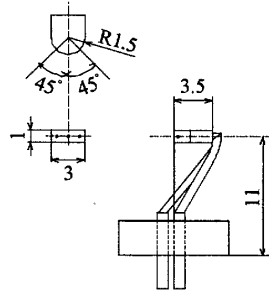
Fig. 2 Test impeller.

Fig. 3 Head geometry of cobra-type three-holes yaw-meter.

impeller shroud side, were measured continuously with sensors[7], whose response frequency is about 1 kHz. Here the radius of impeller outlet is denoted as r_2. At three radial sections of $R=1.03$, 1.10 and 1.28, wall pressures at two positions with the circumferential difference of 50 degrees at each radius and were measured simultaneously to evaluate the numbers and rotating speed of the stall cell. In addition of these pressure measurements, flow distributions of the static head h_s, the absolute velocity V and flow angle α from the circumferential direction were measured by using a cobra-type three-holes yaw-meter as shown in **Fig. 3**. The yaw-meter was installed on the diffuser wall of the impeller shroud side. The measured pressure at each hole of the yaw-meter was transferred to the sensor through the connecting pipe, which was filled with a silicone-oil. The response frequency of the pressure measuring system was about 1 kHz. In the present experiment of rotating stall occurring, the flow measurement at six sections in r-direction of $R=1.03$, 1.06, 1.10, 1.15, 1.28, 1.50 and at seven in the z-direction of the blade height was carried out as follows. (1) The yaw-meter was set at one position. (2) The yaw angle was fixed and pressure signals of three-holes were obtained simultaneously and continuously for three seconds of measuring time with the sampling frequency of 300 Hz. (3) The yaw angle was changed every five degrees and fixed for measurement. (4) Measured signals have three components of discrete frequencies, such as blade passing frequency, impeller rotating frequency and the rotating stall frequency, which was obtained from spectrum analysis of the fluctuations. The signals were phase-locked with measured stall frequency or impeller rotating frequency, overlapped and averaged over ten periods of corresponding fluctuation with phase locking. By this procedure, the corresponding frequency component is remained and the other components are diminished. (5) After evaluating flow velocity and static pressure from pressure signals, the data is stored only when the center hole of yaw-meter was oriented to the range within ±45 degrees of flow direction. (6) The same measurement was carried out ten times to obtain reliable data.

In the present paper, the flow coefficient ϕ is denoted as the ratio of averaged radial

velocity component V_{r2} to the impeller rotating velocity U_2 at the just downstream section of impeller outlet. The static head coefficient ψ_s and ψ_{so} as the ratio of the static head rise based on the pump inlet total head and the free-surface pressure head downstream of diffuser outlet to $U_2^2/(2g)$ where g is the acceleration of gravity.

3. Results and Discussions

3.1 Impeller and diffuser characteristics

The static head rise characteristic of impeller is discussed at first. **Figure 4** shows the head rise at $R=1.03$ from impeller inlet total head. The measured theoretical head coefficient $\psi_{t-th}=2\overline{V_{u2}}/U_2$ is denoted as the ratio of the Euler's head with no preswirl at impeller inlet to $U_2^2/(2g)$, where the superscript of "—" means mass-averaged value. The value of ψ_{t-th} is evaluated from measured velocity distributions at $R=1.03$. In **Fig. 4** the following empirical expressions, which are derived from one dimensional flow model, are also depicted as broken lines.

$$\psi_{t-th}=2(0.78-1.04 \cdot \phi/\tan\beta_{b2p}) \tag{1}$$

$$\psi_s=(0.78-1.04\,\phi/\tan\beta_{b2p})[2-(0.78-1.04\,\phi/\tan\beta_{b2p})]-\phi^2 \tag{2}$$

Though the negative slope of measured head rise is gradually weakened as the flow rate is decreased in the range of $\phi<0.1$, the same tendency between measured and empirical results can be seen, which reveals that the rotating stall phenomena in the present experiment depends upon the flow mechanism in the diffuser, not upon the impeller. In fact, the reverse flow in the impeller inlet at low flow rate was not recognized from a flow visualization of the tuft method. The impeller outlet flow at low flow rate consists of the jet and wake regions, the latter of which has low radial velocity and high tangential velocity components and the former has high radial velocity and low tangential velocity. The wake region becomes larger as flow rate is decreased so that the mass-averaged tangential velocity of $\overline{V_{u2}}$ is small. As
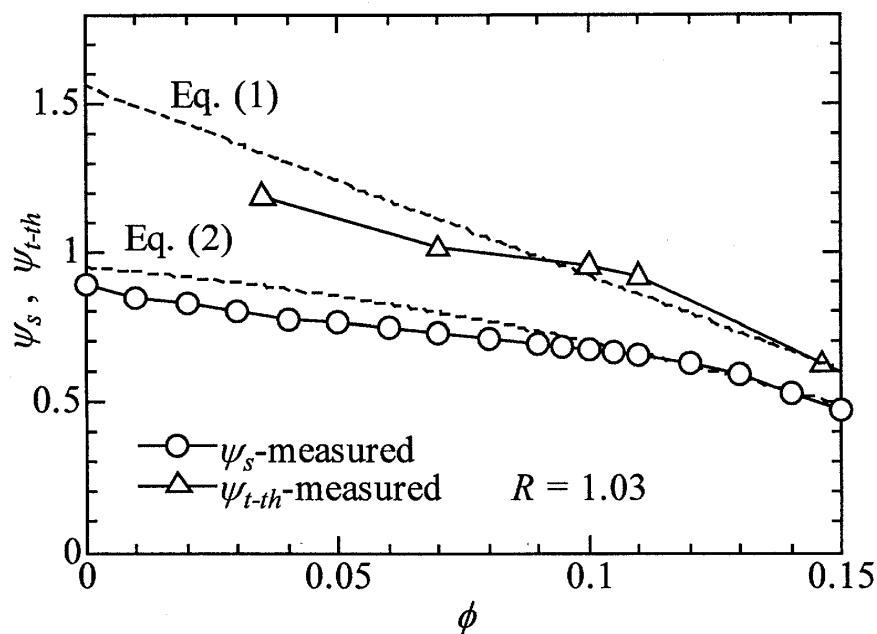

Fig. 4 Head rise characteristics of impeller.

the result, the negative slope of head rise at $\phi<0.1$ might become weak.

Figure 5 shows the radial and tangential velocity distributions of $\overline{V_r}$ and $\overline{V_u}$ in the direction z of diffuser height between hub ($z/b=1$) and shroud ($z/b=0$). The distributions are relatively uniform at this radial position of $R=1.03$ (just downstream of impeller) except for that of $\phi=0.035$, where the reverse flow appears in the shroud side.

Figure 6 shows changes of static head recovery ψ_{so} in the diffuser with flow rate, where $\psi_{so}=0$ means that the head on the free surface of collector of overflow-tank ③ in **Fig. 1**. Assuming that static-head rise of the impeller is given as **Eq.(2)** and static head recovery is decided only from the change of velocity while keeping continuity relation rV_r=constant and angular momentum conservation rV_u=constant, the next expression is derived, results of which are shown as broken lines in **Fig. 6**.

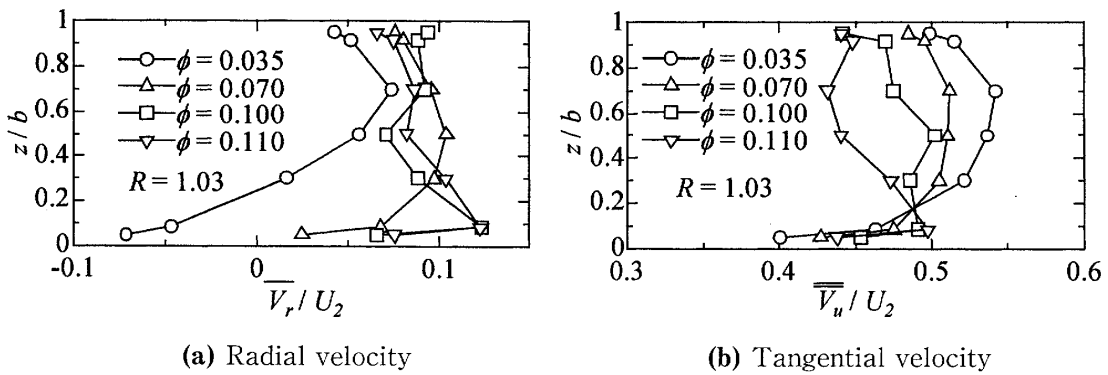(a) Radial velocity   (b) Tangential velocity

Fig. 5 Velocity distribution at impeller outlet.

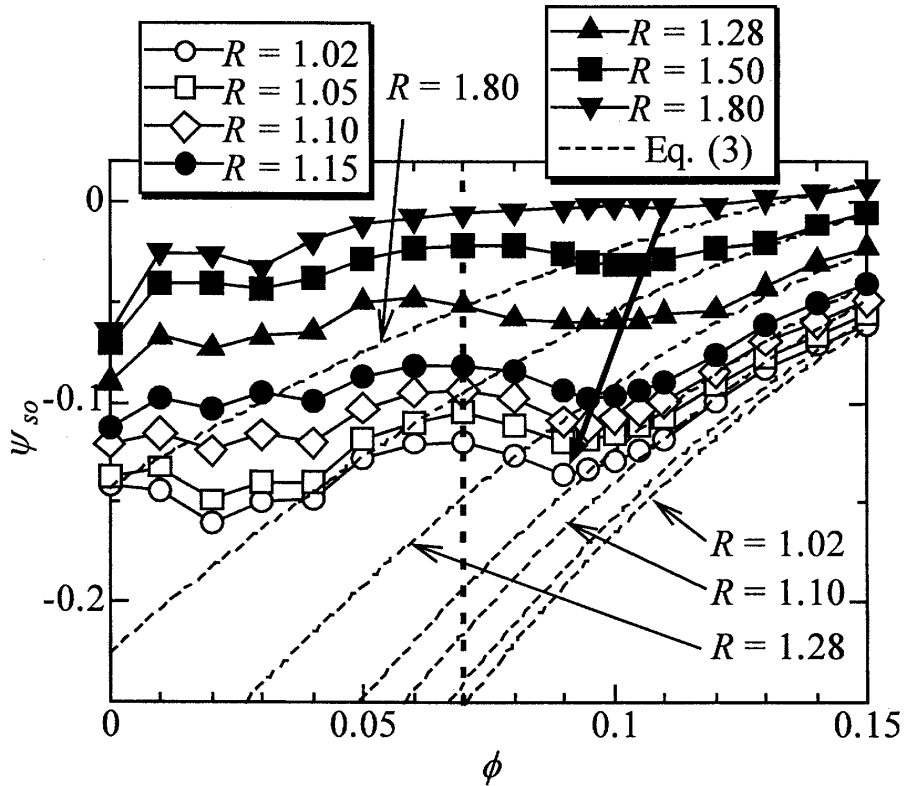**Fig. 6** Static head recovery in radial diffuser.

$$\psi_{so}=0.045-[\phi^2+(0.78-1.04\,\phi/\tan\beta_{b2p})^2]/R^2 \tag{3}$$

According to **Eq.(3)**, static head recovery in the diffuser is increased as flow rate is decreased since the constant value of rV_u becomes larger. Then even at the position of $R=1.8$ tangential velocity still remains large. However, the measured static head recovery is different from the ideal one due to change in flow behavior in the diffuser passage. When flow rate is decreased from $\phi=0.15$ the value of ψ_{so} at the position of constant radius is decreased and takes the minimum. Then with further decrease of flow rate, the value of ψ_{so} once becomes large in the vicinity of $\phi=0.06$ and then gradually decreases. In this characteristic, the flow rate, where the minimum value of ψ_{so} appears, moves from $\phi=0.11$ at $R=1.8$ to $\phi=0.09$ at $R=1.02$ as indicated by an arrow in **Fig. 6**. As a result, the highest degree of static head recovery appears at $\phi=0.09$. As the degree of static head recovery would be related to change in three-dimensional flow pattern, the distributions of V_r component in height direction at $R=1.03$, 1.10 and 1.28 are measured and shown in **Fig. 7**. In the case of $\phi=0.11$ the reverse flow regions are found in hub-side region at $R=1.10$ and 1.28 and not found at $R=1.03$ just downstream of impeller. It is guessed that the reverse flow occurs from the diffuser outlet of large R-position at first and the movement of position with the minimum static head as an arrow line in **Fig. 6** expresses the elongation of the reverse flow region to upstream section. Then in the case of $\phi=0.07$ the reverse flow region in hub side of large R position is weakened. At this flow rate region, the wall shear stress might be stronger due to steep velocity gradient near wall so that friction loss is increased and static head recovery becomes poor. With further decreasing flow rate, the reverse flow region appears again in shroud side, not in hub side as shown in **Fig. 7(c)** except $R=1.10$ where reverse flow appears locally as shown in **Fig. 13**. At low flow rate of $\phi=0.035$, it is presumed
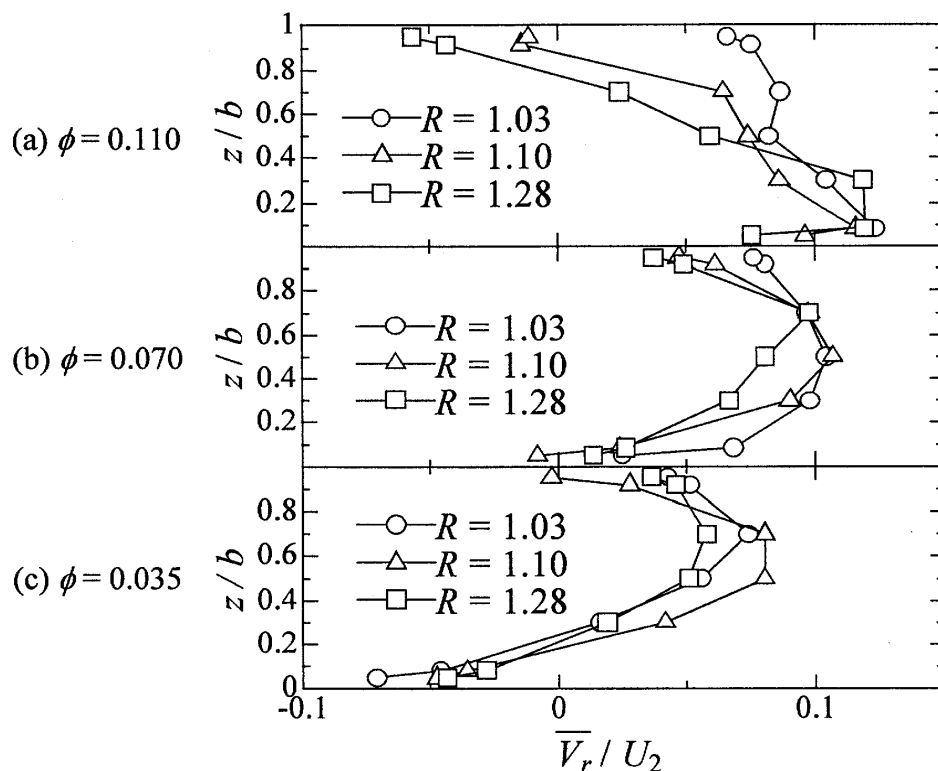

Fig. 7 Distributions of radial velocity component at various radial Positions.

that the reverse flow occurs from the impeller outlet at first.

3.2 Rotating stall behaviors

Figure 8 shows the behavior of free surface in the overflow-tank ③ in **Fig. 1**. While stable surface appears and water axisymmetrically overflows at $\phi > 0.11$ as shown in **Fig. 8(a)**, the rotating wavy motion with low frequency is observed as shown in **Fig. 8(b)**. The appearance of rotating stall cell can be clearly visualized by using water as working fluid different from air.

Examples of measured fluctuations of static head on the shroud casing wall at $R = 1.03$ are shown in **Fig. 9**, where the vertical axis is ψ_{so} and the horizontal one is time of t. The measured head fluctuation inherently has a component of blade passing frequency called as BPF. As flow rate is decreased to $\phi < 0.11$, a wavy motion with low frequency appears in measured head fluctuation due to rotating stall occurring. Spectrum analysis of measured head fluctuations was performed and the results are depicted in **Fig. 10** for measured data at $R = 1.03$. The amplitude of each frequency component of the fluctuation is denoted as $\Delta\psi$ and the frequency of rotating stall is called as SF. The components of BPF and its harmonics are discrete over measured range of flow rate. In addition, an amplitude of low frequency becomes distinguished in flow rate range of $\phi < 0.11$. This component of frequency is recognized as a rotating stall occurring by simultaneous measurement with two sensors located at the same radial but different circumferential positions with 50 degrees.

Figure 11 shows change of rotating stall behaviors with flow rate. It is found from this figure that the rotating stall occurs at $\phi = 0.105$. The absolute flow angle, calculated from $\alpha = \tan^{-1}(\overline{V_r}/\overline{V_u})$, takes 11.9 degrees at $R = 1.03$ and this stall onset angle is an appropriate value in comparison with a predicted value from previous report[8].

Looking at the amplitude of BPF component in **Fig. 11(a)**, the amplitude becomes weakened with increase of radial position as it is known[1] that the outlet flow of impeller becomes almost uniform at radial position of $R > 1.2$. The amplitude of BPF component is also decreased with decrease of flow rate. On the other hand, the amplitude of SF component is larger than that of BPF even at the just downstream position of impeller and the degree of its decay in the downstream direction is not so strong. The frequency of rotating stall, the rotating speed of stall cell in **Fig. 11(b)** and its amplitude gradually increase with decrease in flow rate. In **Fig.11 (b)**, the rotating speed of stall cell are denoted as ω_s, and Ω means the rotational speed of the impeller. In the present experiment the number of stall cell of n

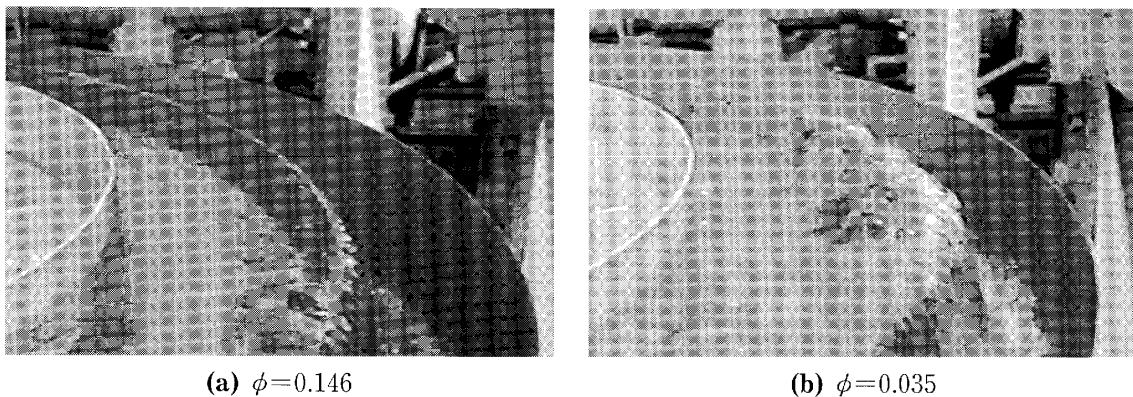(a) $\phi = 0.146$ (b) $\phi = 0.035$
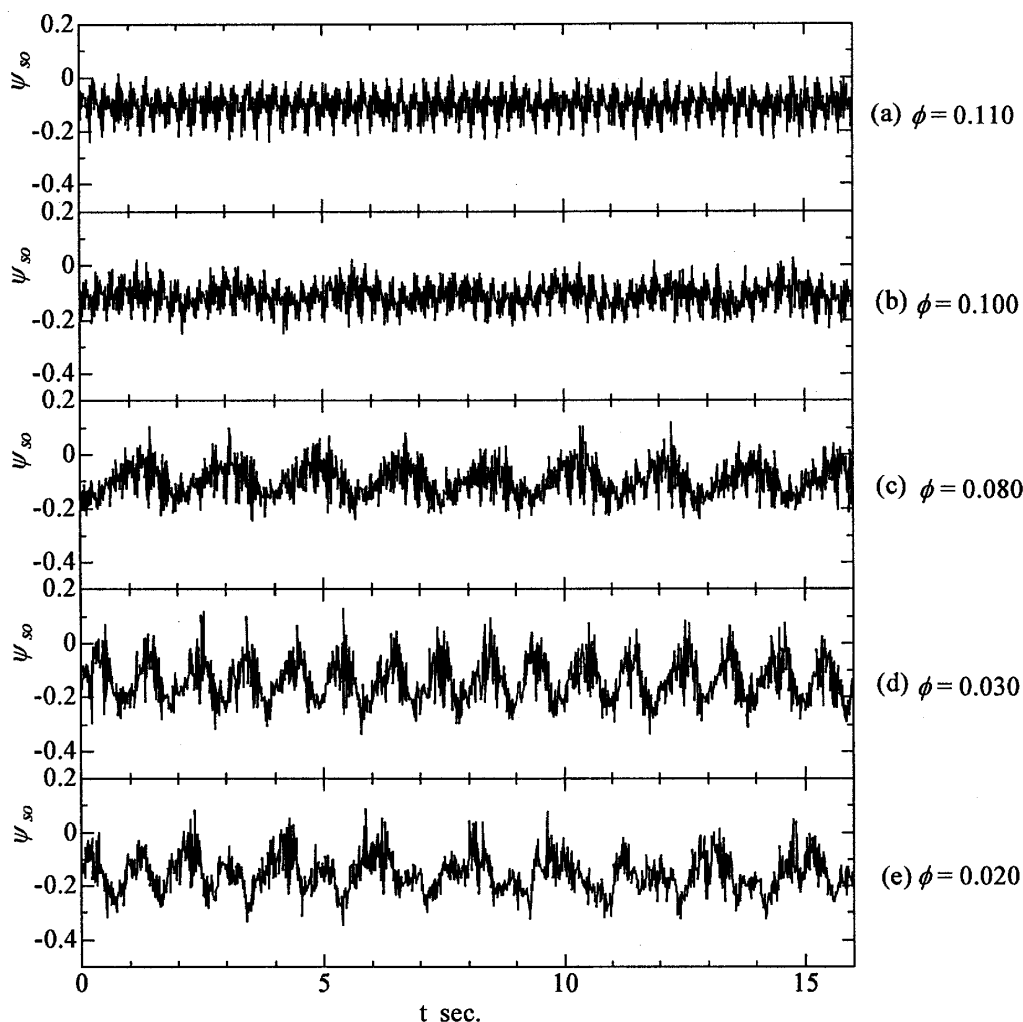
Fig. 8 Observed wavy motion of free surface of collector.
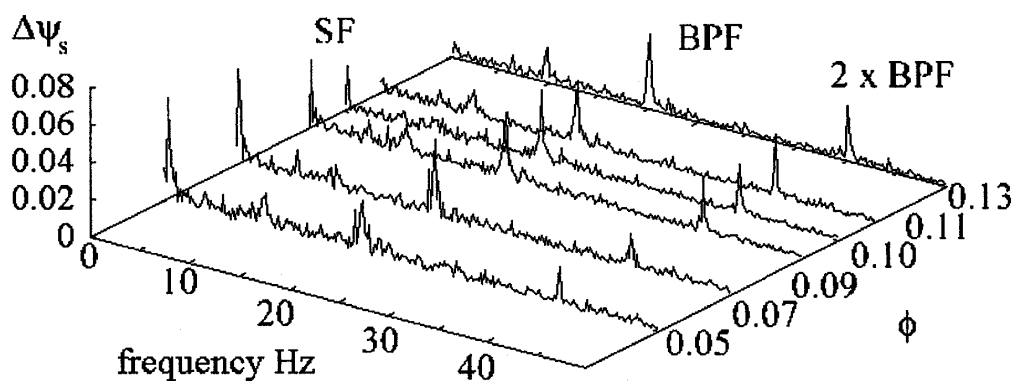
Fig. 9　Time variation in measured static head.

Fig. 10　Spectrum analysis of measured static head fluctuations at $R=1.03$.

is calculated as two in the range of $\phi < 0.10$ from static head measurement with two sensors, which is also found from free-surface observation as shown in **Fig. 8(b)**. As can be seen from **Fig. 9(e)**, the static head fluctuation becomes more complicated at extremely lower flow rate of $\phi < 0.02$. In this range of ϕ, one cell of rotating stall also appears as alternate phase of two cells.
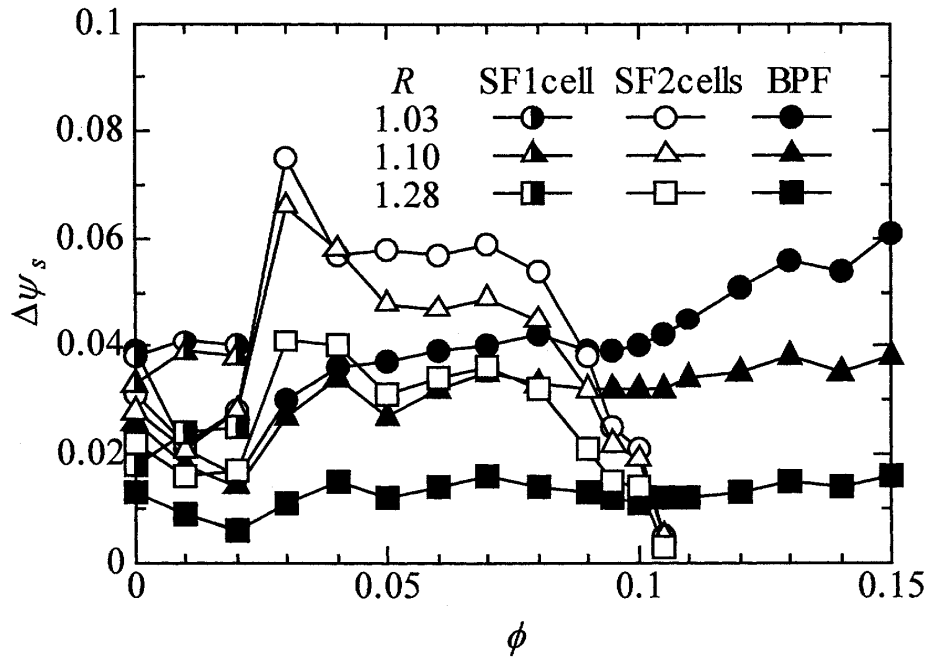
(a) Amplitude of SF and BPF components
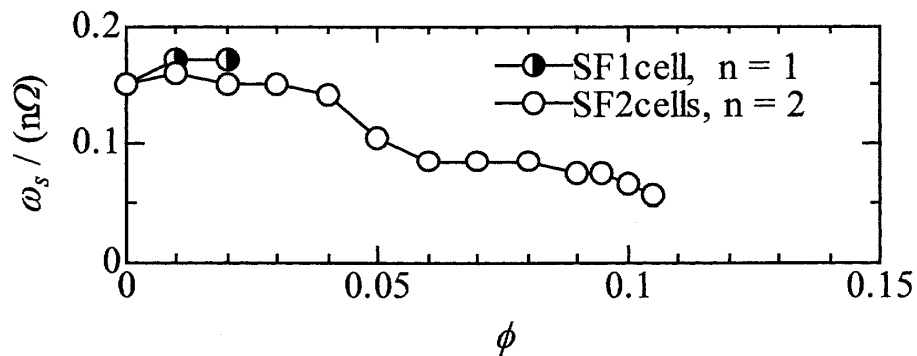
(b) Rotating stall frequency and rotating speed of stall cell

Fig. 11 Change of rotating stall behaviors with flow rate.

Figures 12 and 13 show the rotating stall behavior at $\phi = 0.035$ by using contour maps of flow distributions near the shroud wall ($z/b = 0.05$) and the hub wall ($z/b = 0.95$) respectively, where ψ_t and ψ_s are total and static head rise coefficients from the impeller inlet, V absolute velocity, α flow angle. A negative value of α means that the flow is inward, i.e. a reverse flow. The flow distribution on the shroud side of $z/b = 0.05$ where a reverse flow appears over a whole zone is depicted in Fig. 12 and on the hub side of $z/b = 0.95$ where a normal flow appears in Fig. 13. Nevertheless the normal and reverse flows are clearly divided at this flow rate of $\phi = 0.035$, the static head distributions in both sides are almost the same and independent of height direction z; i.e. the pressure distribution is two dimensional. A zone of higher static head recovery reveals lower velocity with low flow angle while that of lower recovery reveals higher velocity with high angle. As a zone of higher total head appears in the higher velocity zone, water might overflow as shown in Fig. 6(b) from this higher total head zone of the channel ③ in Fig. 1.
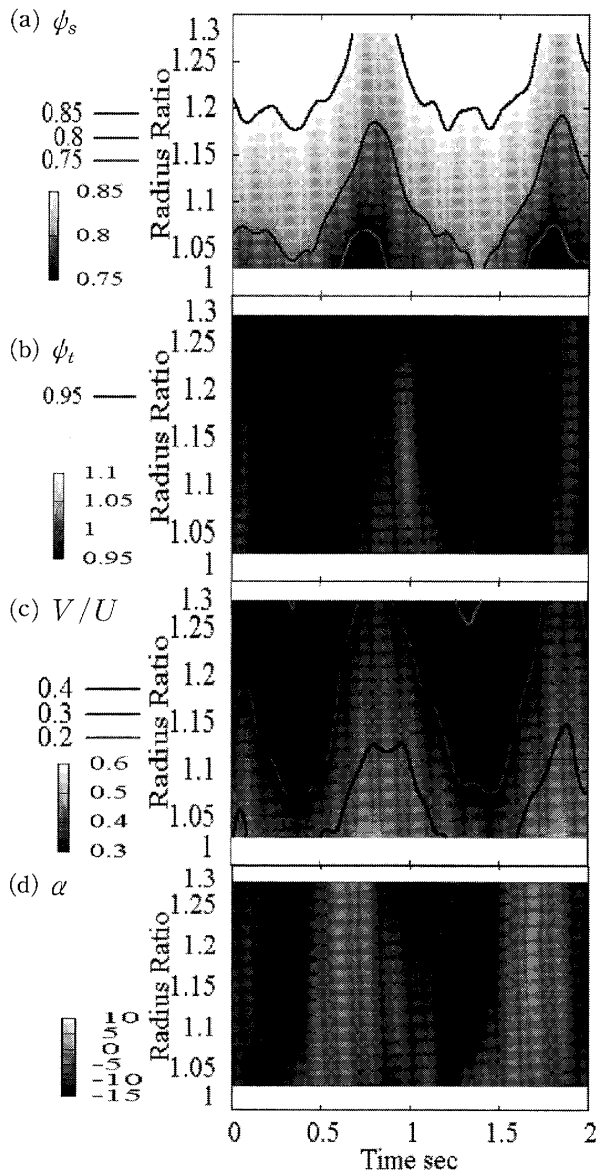
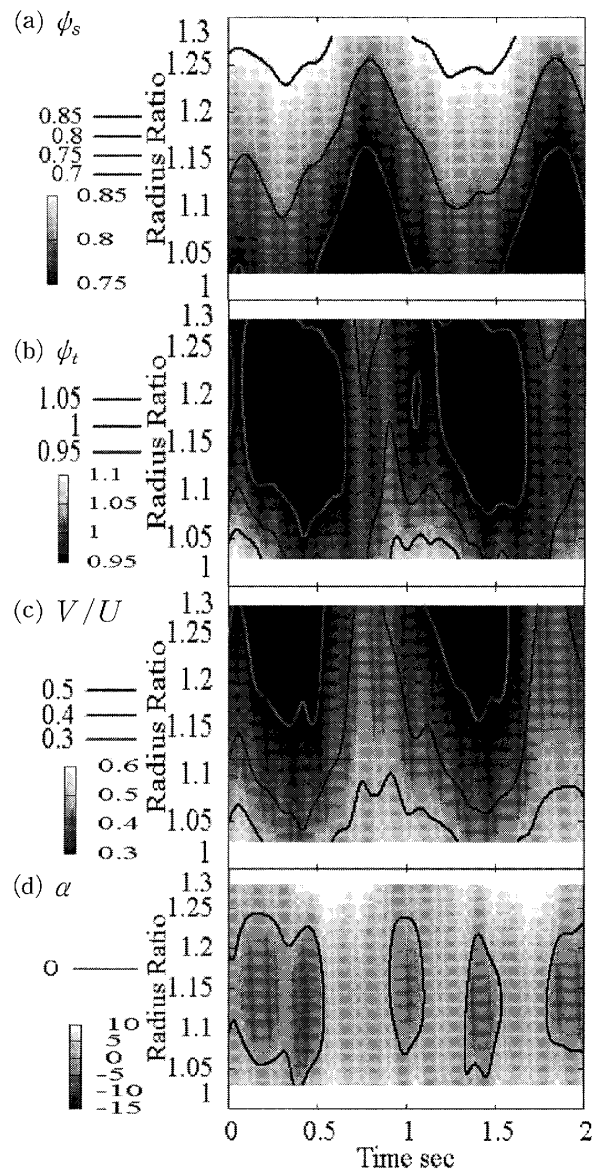**Fig. 12** Rotating stall behavior at $\phi=0.035$ and $z/b=0.05$ (shroud side).

Fig. 13 Rotating stall behavior at $\phi=0.035$ and $z/b=0.95$ (hub side).

Figures **14** and **15** show the rotating stall behavior at $\phi=0.10$ in the same manner as **Fig. 12**. At this flow rate a reverse flow appears near the hub side, only in $R>1.10$ as shown in **Fig. 15**, which is different from the case of $\phi=0.035$. The reverse flow zone also reveals higher static head recovery and lower velocity. In the shroud side as shown in **Fig. 14**, the distribution of static head recovery is almost the same one as that in the hub side. However as there is a normal flow in a whole zone in this shroud side, the flow structure of rotating stall cell becomes obscure.

4. Conclusions

A rotating stall phenomenon in radial vaneless diffuser of centrifugal pump has been investigated experimentally as the first stage of developing a method to suppress the stall. The results are summarized as follows.
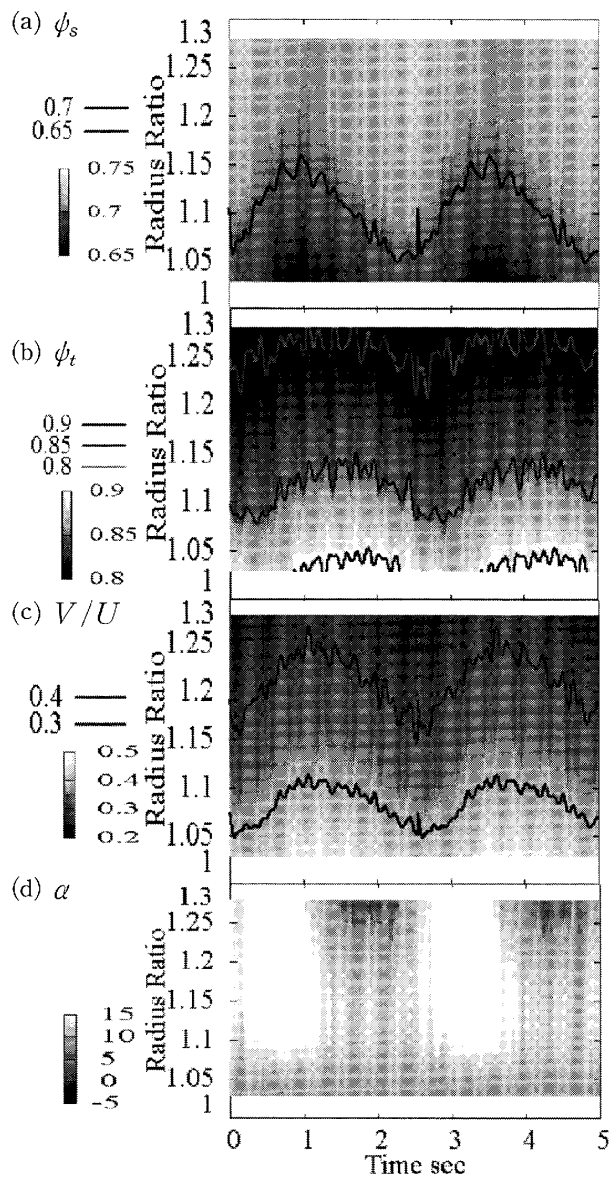
Fig. 14 Rotating stall behavior at ϕ=0.10 and z/b=0.05 (shroud side).
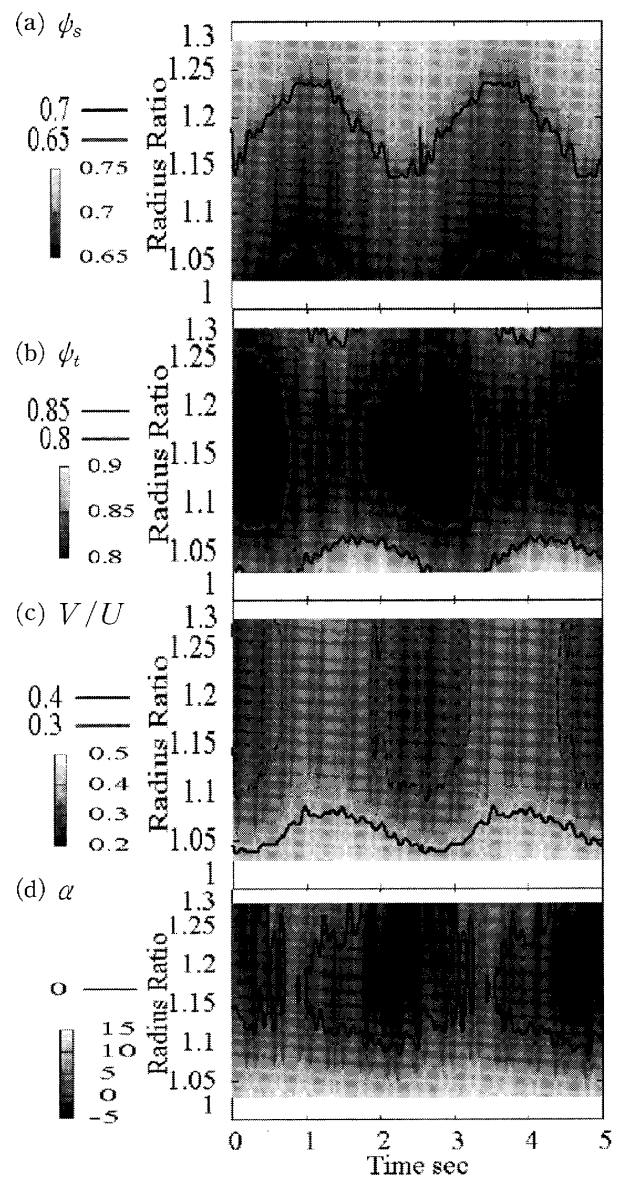
Fig. 15 Rotating stall behavior at ϕ=0.10 and z/b = 0.95 (hub side).

(1)   The appearance of rotating stall is closely related to a reverse flow occurring in the diffuser. At higher flow rate the reverse flow occurs on the hub surface near the diffuser outlet when the average angle of absolute flow velocity becomes less than about 12 degrees at the just downstream section of the impeller. At lower flow rate, a reverse flow occurs as the interaction between the diffuser and the impeller.

(2)   The rotating stall behaviors have been clarified against a combination of test impeller and diffuser. The number of stall cells is two and flow passage in the diffuser is divided into two zones. One reveals low static head, high velocity, high total head and small flow angle even in a reverse flow region. The other reveals high static head, low velocity, low total head and negatively large flow angle.

References

1) Furukawa. A., Takahara. H., Nakagawa. T., Downstream Flow of Centrifugal Pump Impellers in Vaneless Diffuser with Parallel Walls, *Mem. Fac. Eng., Kyushu Univ.*, 60-2, (2000), 21-33.

2) Jansen, W., Rotating Stall in a Radial Vaneless Diffuser, *Trans. ASME, Journal of Basic Engineering*, (1964), 750-758.

3) Ishida, M., Sakaguchi, D., Ueki, H., Suppression of Rotating Stall by Wall Roughness Control in Vaneless Diffusers of Centrifugal Blowers, *Trans. ASME, Journal of Turbomachinery*, Vol.123, (2001), 64-72.

4) Kurokawa, J., Sankar, L. S., Matsui, J., Kitahora, T., Passive Control of Rotating Stall in a Parallel-Wall Vaneless Diffuser by Radial Grooves, *Trans. ASME, Journal of Fluids Engineering*, Vol.122, (2000), 90-96.

5) Yoshida, Y., Tateishi, T., Tsurusaki, H., Tsujimoto, Y., Active Control of Vaneless Diffuser Rotating Stalls, *Trans. JSME*, (in Japanese), 58-554, (1992), 3067-3073.

6) Tsurusaki, H., Kinoshita, T., Flow Control of Rotating Stall in a Radial Vaneless Diffuser, *Trans. ASME, Journal of Fluids Engineering*, Vol.123, (2001), 281-286.

7) Takahara, H., Takamatsu, Y., Kouno, I. and Kurahara, T., A Study on Flow Measurement Scheme by Stepwise Rotation of Total-Pressure Tube in Flow with Steep Velocity and Pressure Gradients, *Trans. JSME*, (in Japanese), 55-510, B(1989), 413-418.

8) Senoo, Y., Kinoshita, Y., Influence of Inlet Flow Conditions and Geometries of Centrifugal Vaneless Diffusers on Critical Flow Angle for Reverse Flow, *Trans. ASME, Journal of Fluids Engineering*, Vol.99, (1977), 98-103.